Supplementary Information

Highly dispersive Co_3O_4 nanoparticles incorporated in a cellulose nanofiber for a high performance flexible supercapacitor

Iqra Rabani[a], Jeseung Yoo[a], Hyo-Sun Kim[a], Do Van Lam[b], Sajjad Hussain[a], K. Karuppasamy[c] and Young-Soo Seo[a]*

[a]Department of Nanotechnology and Advanced Materials Engineering, Sejong University, Seoul 05006, Republic of Korea.

[b]Department of Applied Nanomechanics, Korea Institute of Machinery and Materials, Daejeon 34103, Republic of Korea

[c]Division of Electronics and Electrical Engineering, Dongguk University-Seoul, Seoul 04620, Republic of Korea.

*Corresponding author: Prof. Young-Soo Seo; E-mail: ysseo@sejong.ac.kr

Content

S1. Characterizations

Figure S2. Elemental mapping for the 1D Co3O4@CNF hybrid.

Figure S3. Cyclic voltammetry (CV) at different scan rates using 3 M KOH electrolyte within voltage window from -0.2 V to +0.6 V for **(a)** 1D Co_3O_4@CNF1 hybrid, **(b)** 1D Co_3O_4@CNF3 hybrid.

Figure S4. Charging/discharging (GCD) curves at current densities for **(a)** 1D Co_3O_4@CNF1 hybrid and **(b)** 1D Co_3O_4@CNF3 hybrid.

Figure S5. CV curves using 3 M KOH electrolyte at different scan rates within voltage window from -0.2 V to +0.6 V of **(a)** pristine Co_3O_4 nanoparticles **(b)** pristine CNF.

Figure S6. GCD curves at current densities with voltage window from -0.2 V to +0.6 V for **(a)** pristine Co_3O_4 nanoparticles **(b)** pristine CNF.

Figure S7. CV curves using 3 M KOH electrolyte at different scan rates within voltage window from 0 V to 1 V of **(a)** pristine Co_3O_4 nanoparticles and **(b)** pristine CNF.

Figure S8. GCD curves at current densities with voltage window from 0 V to 1 V for **(a)** pristine Co_3O_4 nanoparticles and **(b)** pristine CNF.

Figure S9. Energy density with respect to the power density plot at the different current sweep rates.

S10. Energy density and power density calculations by the non-linear discharging curve

Figure S11. Ragone plot using integrated discharging formula.

Figure S12(a-b). FESEM images of the 1D Co_3O_4@CNF flexible paper like film.

Figure S13. EDX spectrum of the 1D Co_3O_4@CNF flexible paper like film.

Figure S14. Stability curve of the 1D Co_3O_4@CNF flexible paper over the 50^{th} cycle at the bending state.

Table S1. Comparative Electrochemical Performance of 1D Co_3O_4@CNF in the Three-Electrode System with Other Previously Reported Materials.

Table S2. Comparative Electrochemical Performance of 1D Co_3O_4@CNF in the Two-Electrode System with Other Previously Reported Symmetric and Asymmetric Materials.

References

S1. Characterizations

The surface morphology of the as prepared (1D Co_3O_4@CNF hybrid, CNF and Co_3O_4) was analyzed using field emission scanning electron microscopy (FESEM; (JEOL JSM-6700F)) and transmission electron microscopy (TEM; (FEI Tecnai F30 S-TWIN TEM)). To TEM, sample were prepared by means of adding few drops of ethanol with samples and ultrasonically sonicated for about 1 min. Then, 0.3 µ/ml was dropped over carbon grid and arid into the vacuum oven for 1 hour. Compositional analysis was performed by using energy dispersive X-rays (EDX) technique operating at 5 kV and 10 keV. The sample was prepared for the EDX analysis by means of adding 0.3 µ/ml of diluted sample on the aluminum sheet and dried into the vacuum oven. X-ray diffraction (XRD; D/Max-2550 PC Rigaku Co., Korea, Cu Kα, λ = 1.5406 Å) and Raman spectroscopy (in Via-Reflex, Renishaw, Co., South Korea) analyses were employed to study the crystallinity structure and phase of all samples. X-ray photoelectron spectroscopy (XPS) were carried out using a Thermo Scientific ESCALAB 250Xi X-ray source to obtain the elemental composition, respectively. Moreover, the surface properties were measured using the Brunauer–Emmett–Teller (BET) N_2 adsorption-desorption isotherm by an automated adsorption system (ASAP-2020). The samples were first degassed followed by preconditioning the samples at 150 ºC for 3 hours for the BET analysis. The powder sample was used for all techniques except of the EDX and TEM analyses.

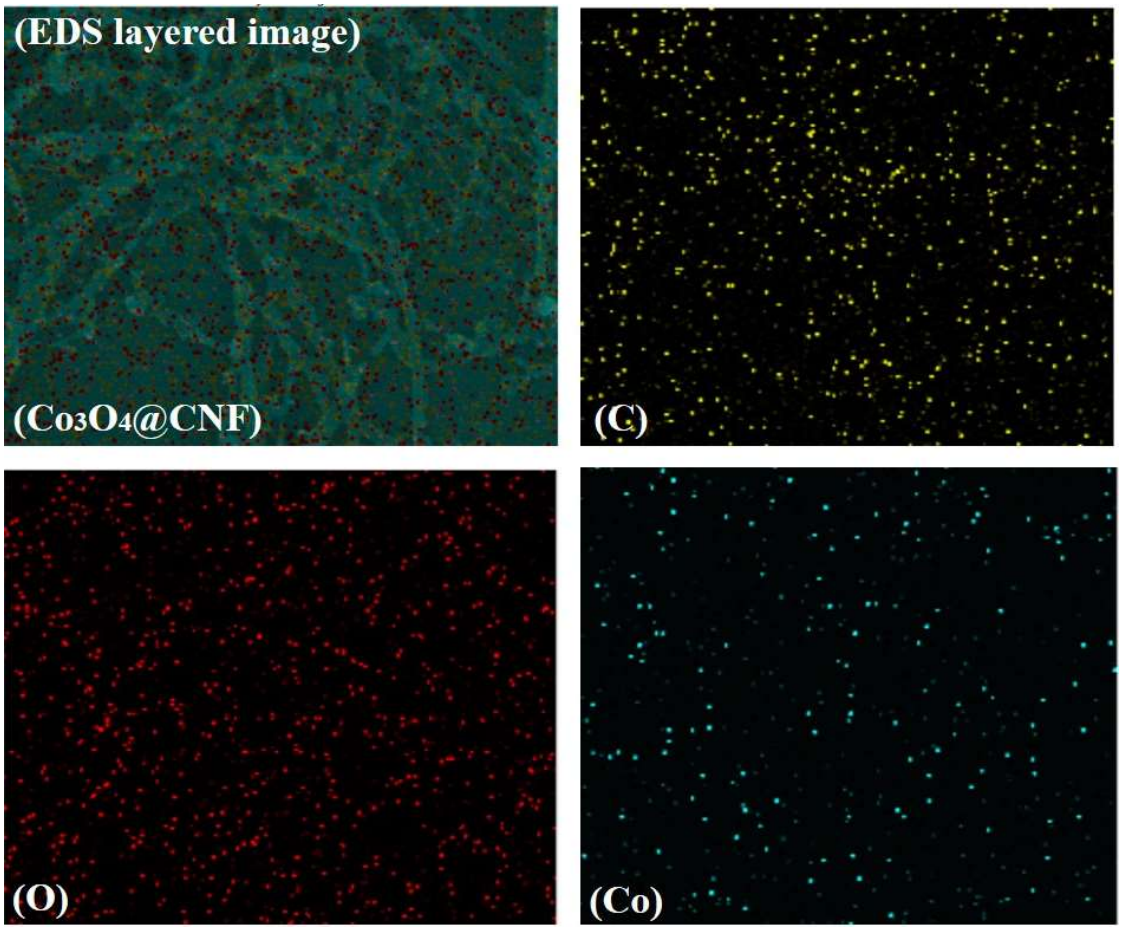

Figure S2. Elemental mapping for the 1D Co3O4@CNF hybrid.

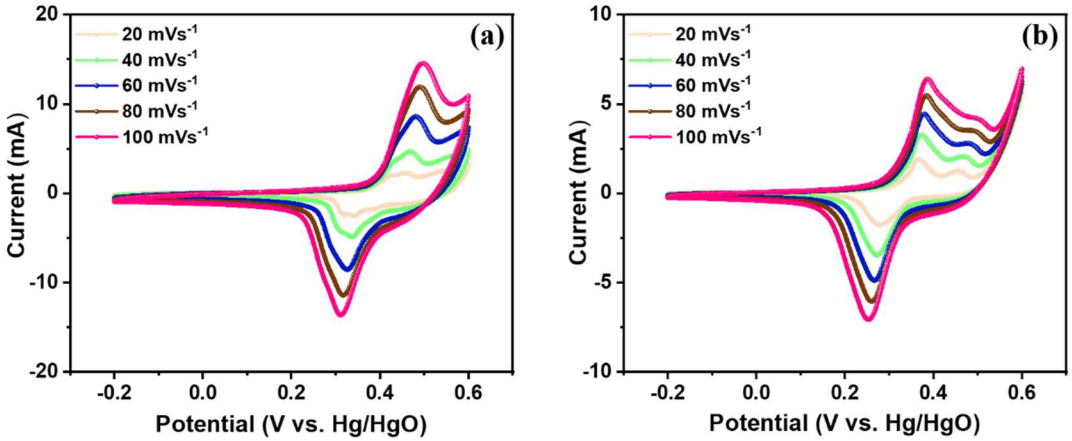

Figure S3. Cyclic voltammetry (CV) at different scan rates using 3 M KOH electrolyte within voltage window from -0.2 V to +0.6 V for **(a)** 1D Co_3O_4@CNF1 hybrid, **(b)** 1D Co_3O_4@CNF3 hybrid.

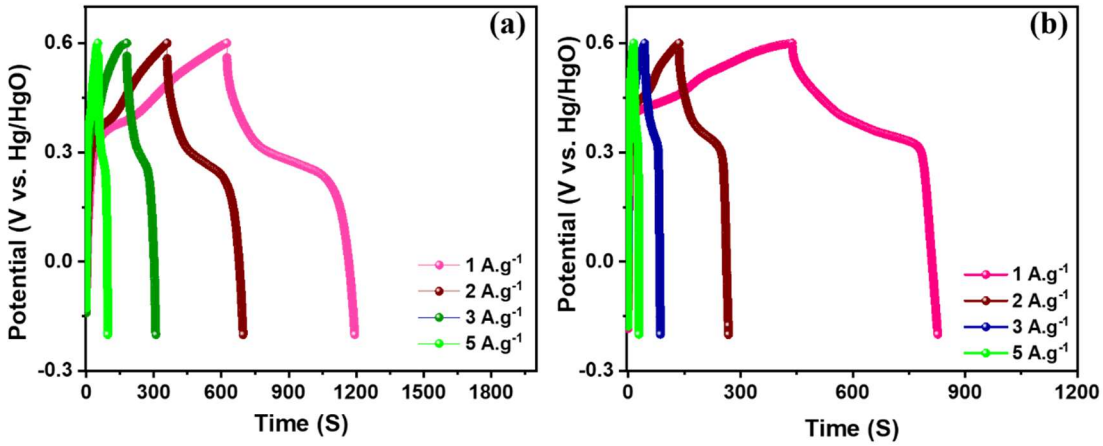

Figure S4. Charging/discharging (GCD) curves at current densities for **(a)** 1D Co_3O_4@CNF1 hybrid and **(b)** 1D Co_3O_4@CNF3 hybrid.

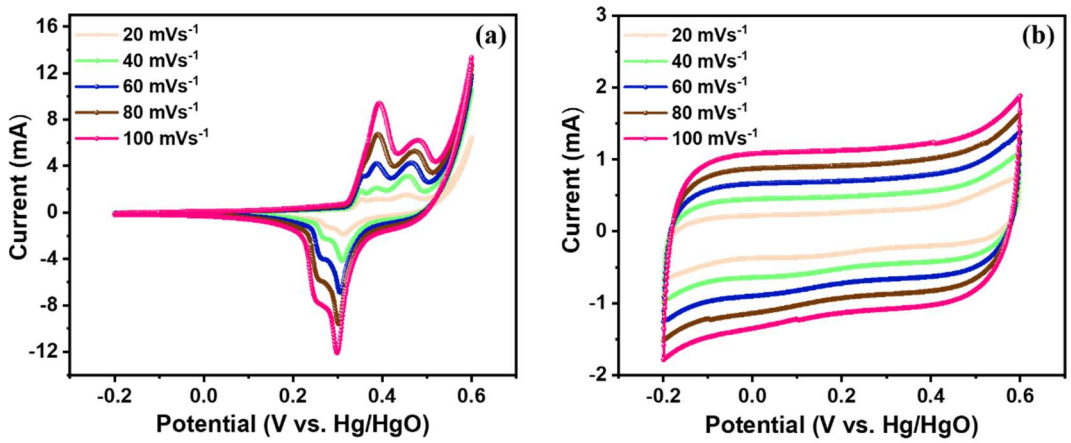

Figure S5. CV curves using 3 M KOH electrolyte at different scan rates within voltage window from -0.2 V to +0.6 V of **(a)** pristine Co_3O_4 nanoparticles **(b)** pristine CNF.

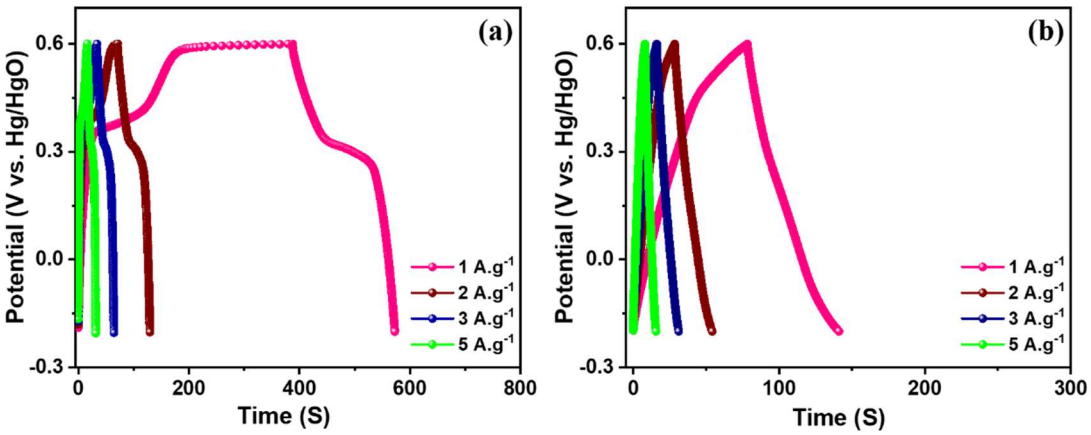

Figure S6. GCD curves at current densities with voltage window from -0.2 V to +0.6 V for **(a)** pristine Co_3O_4 nanoparticles **(b)** pristine CNF.

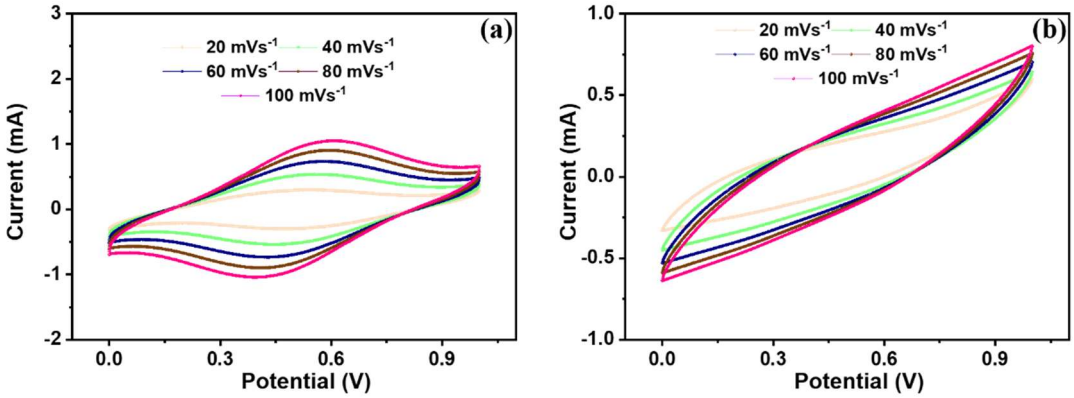

Figure S7. CV curves using 3 M KOH electrolyte at different scan rates within voltage window from 0 V to 1 V of **(a)** pristine Co_3O_4 nanoparticles and **(b)** pristine CNF.

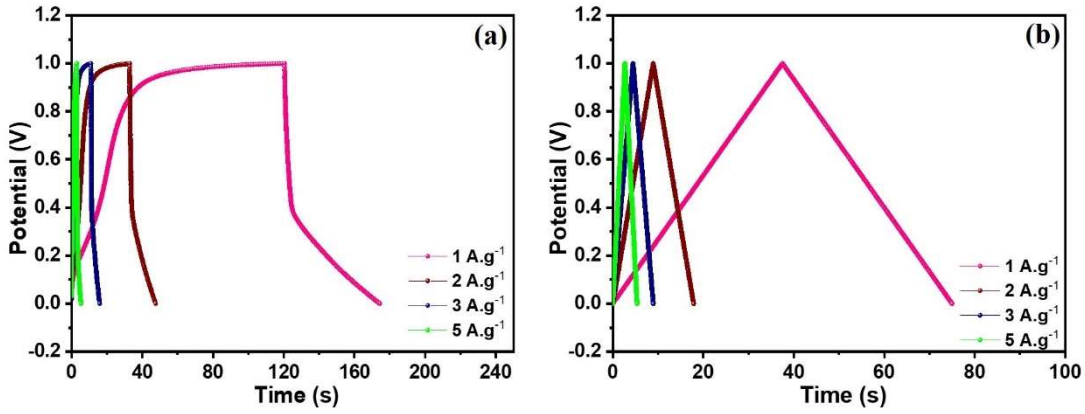

Figure S8. GCD curves at current densities with voltage window from 0 V to 1 V for **(a)** pristine Co_3O_4 nanoparticles and **(b)** pristine CNF.

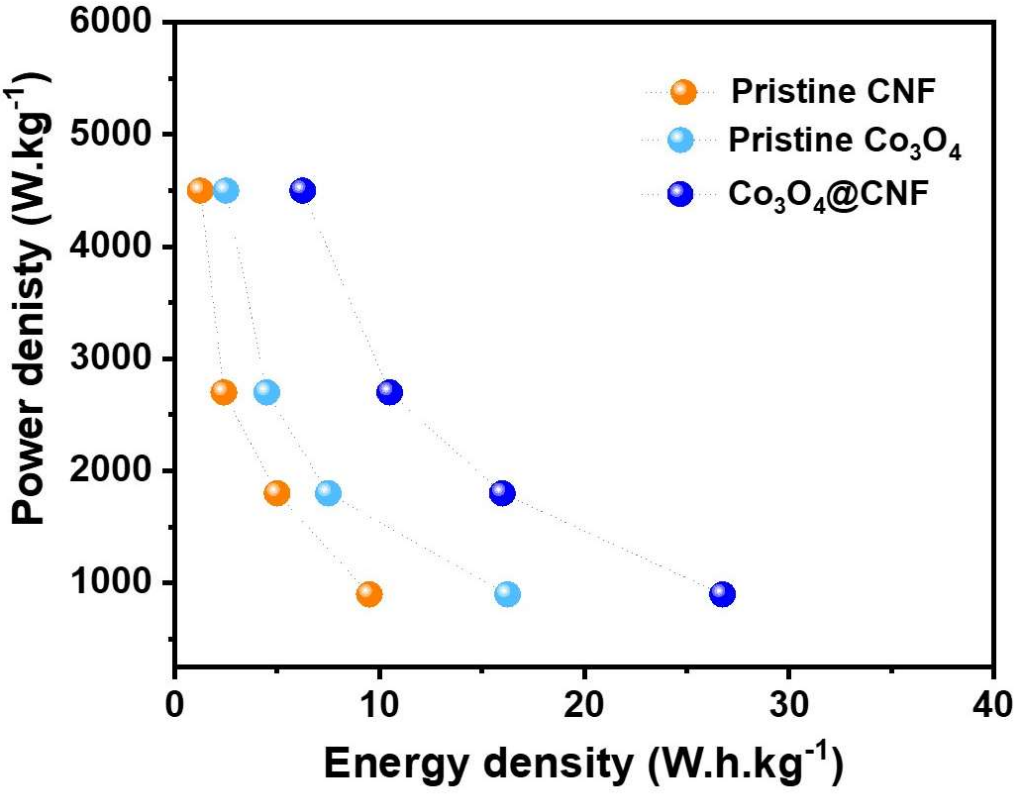

Figure S9. Energy density with respect to the power density plot at the different current sweep rates.

S10. Energy density and power density calculations by the non-linear discharging curve

The energy density (E), and power density (P) of SSCs cells were determined using the following equations:

$E = \frac{1}{m}\int_0^{t_d} iVdt$ ---------- Equation 1

$P = \frac{E}{t_d}$ ---------- Equation 2

Where ΔV is the voltage window, m is the mass of active electrode material, t_d is the discharging time, and i is the loading current density. We investigated the Ragone plot using the integrated discharging curve as can be seen below.

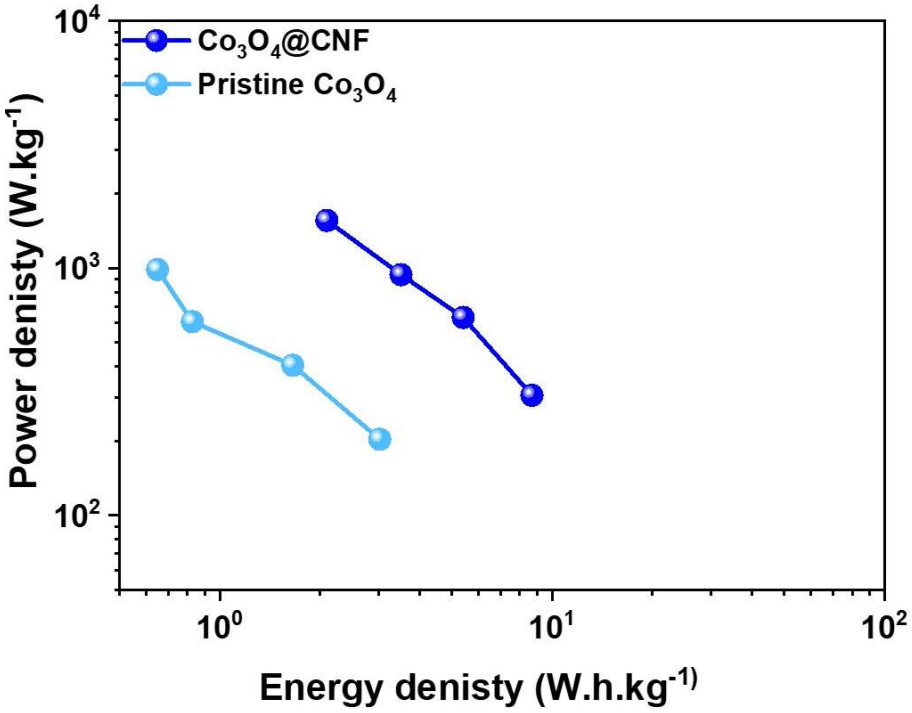

Figure S11. Ragone plot using integrated discharging formula.

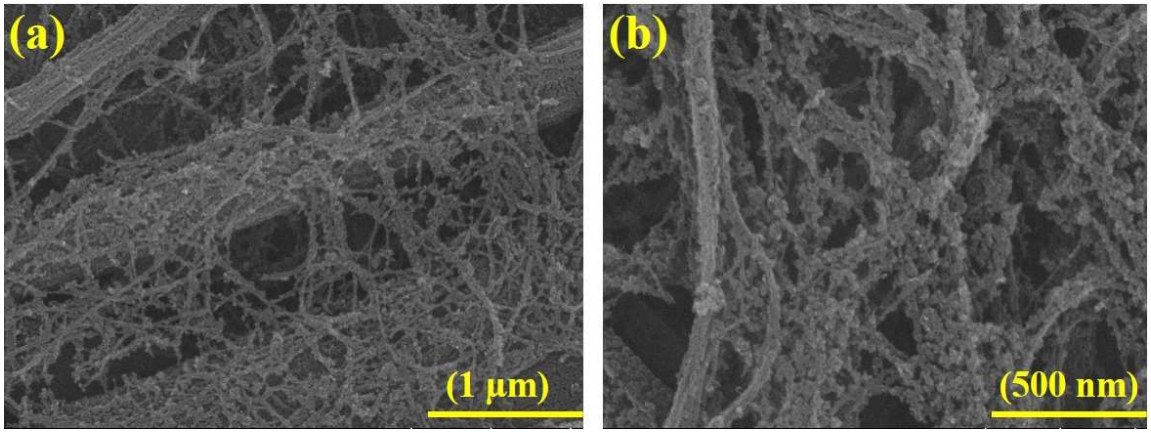

Figure S12(a-b). FESEM images of the 1D Co_3O_4@CNF flexible paper like film.

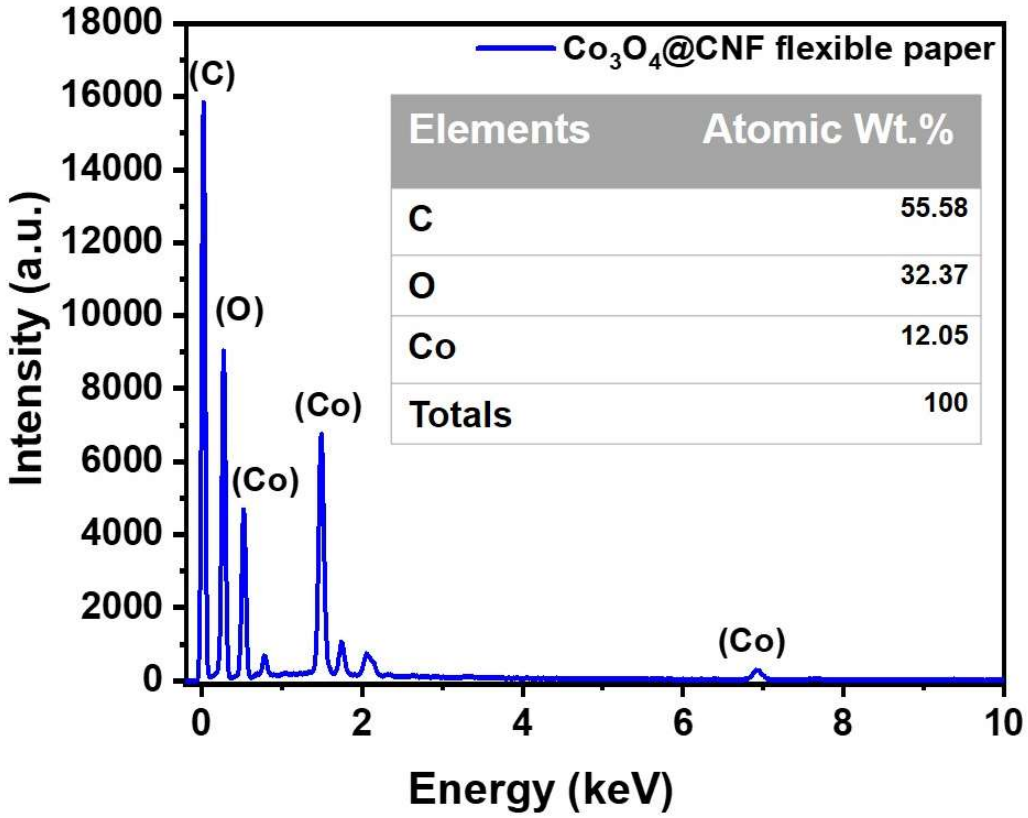

Figure S13. EDX spectrum of the 1D Co_3O_4@CNF flexible paper like film.

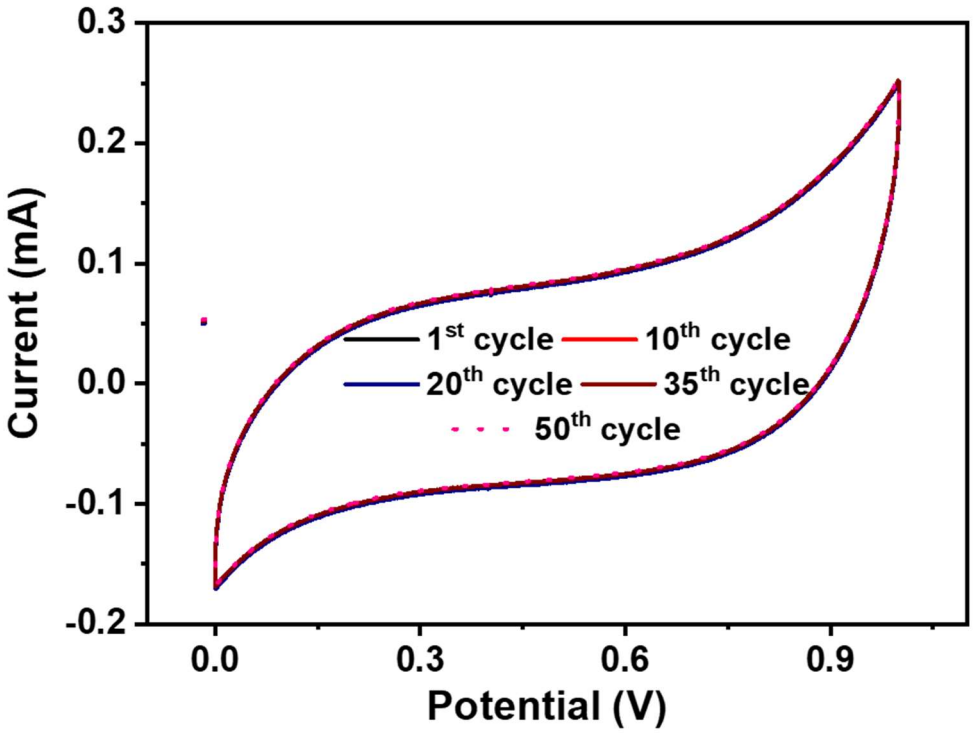

Figure S14. Stability curve of the 1D Co_3O_4@CNF flexible paper over the 50th cycle at the bending state.

Table S1. Comparative Electrochemical Performance of 1D Co_3O_4@CNF in the Three-Electrode System with Other Previously Reported Materials.

Electrode materials	**Voltage window**	**Electrolyte**	**Specific capacitance**	**Ref.**
1D Co_3O_4@CNF	-0.2 to 0.6 V	3 M KOH	789 $F \cdot g^{-1}$ at 1 $A \cdot g^{-1}$	present
yolk shell-$CuCo_2Se_4$	-0.2 to 0.5 V	3 M KOH	512 $F \cdot g^{-1}$ at 1 $A \cdot g^{-1}$	[1]
Co_3O_4 nanocrystals	-0.2 to 0.6 V	6 M KOH	284 $F \cdot g^{-1}$ at 1 $A \cdot g^{-1}$	[2]
Mn-Co sulfide nano sheets	0 to 0.65 V	2 M KOH	1.724 F cm^{-2} at 1 mA cm^{-2}	[3]
Porous $MnCo_2O_{4.5}$	-0.2 to 0.6 V	2 M KOH	342 $F \cdot g^{-1}$ at 0.5 $A \cdot g^{-1}$	[4]
porous Co_3O_4	0 to 0.43 V	3 M KOH	342.1 $F \cdot g^{-1}$ at 1 $A \cdot g^{-1}$	[5]
Co_9S_8@N−C@MoS_2	0 to 0.6 V	3 M KOH	410 $F \cdot g^{-1}$ at 1 $A \cdot g^{-1}$	[6]
Co_3O_4@N-rGO	-0.1 to 0.4 V	3 M KOH	450 $F \cdot g^{-1}$ at 1 $A \cdot g^{-1}$	[7]
$NiCo_2S_4$	0 to 0.6 V	1 M KOH	464 $F \cdot g^{-1}$ at 1 $A \cdot g^{-1}$	[8]
$NiCo_2O_4$	0 to 0.6 V	1 M KOH	173 $F \cdot g^{-1}$ at 1 $A \cdot g^{-1}$	[9]
MnO_2/$MnCo_2O_4$	0 to 0.6 V	2 M KOH	497 $F \cdot g^{-1}$ at 1 $A \cdot g^{-1}$	[10]
NCA/Co_3O_4	-0.05 to 0.45 V	6 M KOH	616 $F \cdot g^{-1}$ at 1.2 A	[10]
$CuCo_2S_4$/CNT/graphene	0 to 0.6 V	1 M Na_2SO_4	504 $F \cdot g^{-1}$ at 10 $A \cdot g^{-1}$	[11]
CPSC-3rGO	-0.2 to 0.8 V	0.2 M Na_2SO_4	446 $F \cdot g^{-1}$ at 1 $A \cdot g^{-1}$	[12]
Co_9S_8@Ni $(OH)_2$	0 to 0.5 V	6 M KOH	149.44 mA h g^{-1} at 1Ag $^{-1}$	[13]
CoS_x@carbon core−shell	0 to 0.4 V	6 M KOH	496 $F \cdot g^{-1}$ at 0.5 $A \cdot g^{-1}$	[14]
petal-like cobalt selenide	−0.1 to 0.65 V	2 M KOH	294 $F \cdot g^{-1}$ at 0.5 $A \cdot g^{-1}$	[15]
Co_3O_4 nanoflakes@SrGO	-0.2 to 0.5 V	2 M KOH	406 $F \cdot g^{-1}$ at 1 $A \cdot g^{-1}$	[16]
$CoMoO_4$ nanoclusters	−0.9 to 0.6 V	6.0 M KNO_3	367 $F \cdot g^{-1}$ at 1.2 $A \cdot g^{-1}$	[17]
Ni-Co selenide	0 to 0.6 V	6 M KOH	742.4 $F \cdot g^{-1}$ at 1 mA cm^{-2}	[18]
$NiCo_2O_4$	-0.2 to 0.6 V	6 M KOH	225 C. g^{-1} at 0.5 A g^{-1}	[19]

Table S2. Comparative Electrochemical Performance of 1D Co_3O_4@CNF in the Two-Electrode System with Other Previously Reported Symmetric and Asymmetric Materials.

Electrode materials	**Type**	**Electrolyte**	**Specific capacitance**	**Capacitance retention (%)/cycles**	**Ref.**
Co_3O_4@CNF	Symmetric	3.0 M KOH	214 $F \cdot g^{-1}$ @ 1.0 $A \cdot g^{-1}$	94/5000	Present
CoNW/CF//CoNW/CF SSC	Symmetric	3.0 M KOH	517.33 mF/cm^3 @ 0.26 mA/cm^2	95/5000	[20]
NCOs	Symmetric	1.0 M KOH	89 F g^{-1} @ 0.23 $A.g^{-1}$	-	[21]
CNF-RGO	Symmetric	H_2SO4-PVA	203 F g^{-1} @ 0.7 mA/cm^2	99/5000	[22]
ZnO/Co_3O_4-450//AC	Asymmetric	1.0 M KOH	153 F g^{-1} @ 1 $A.g^{-1}$	-	[23]
CC@NiC_2O_4 //CC@NC	Asymmetric	6.0 M KOH	89.7 F g^{-1} @ 1 A g^{-1}	86.7/20000	[24]
Co_3O_4@Ni_3S_2	Asymmetric	3.0 M KOH	126 F g^{-1} @ 1 $A.g^{-1}$	83.5/5000	[25]
Ag/NiO	Asymmetric	3.0 M KOH	204 $C.g^{-1}$ @ 2.5 $A.g^{-1}$	96/4000	[26]
Co_3O_4@Ni(OH)2//AC	Asymmetric	6.0 M KOH	110 $F.g^{-1}$ @ 2.5 $A.g^{-1}$	86/1000	[27]
3D graphene-MoS_2 hybrid	Symmetric	KOH/PVA	58.0$F.g^{-1}$@ 2 $A.g^{-1}$	-	[28]
TaS_2	Symmetric	PVA/LiCl	508 F/cm^3 @ 10 mV/s	92/4000	[29]
Cu_2WS_4	Symmetric	PVA/LiCl	583.3 F cm^{-3} @ 0.31 A cm^{-3}	95/3000	[30]
MoS_2-NH_2/PANI nanosheets	Symmetric	1 M H_2SO_4	58.6 F g^{-1} @ 2 $A.g^{-1}$	96.5/10000	[31]
MoS_2/CNS	Symmetric	1 M Na_2SO_4	108 F g^{-1} @ 1 $A.g^{-1}$	-	[32]
MoS_2/G nanobelts	Symmetric	1 M Na_2SO_4	278.2 $F.g^{-1}$ @ 0.8 $A.g^{-1}$	-	[33]

MoS_2/rGO	Symmetric	1 M H_2SO_4	306 $F.g^{-1}$ @ 0.5 $A.g^{-1}$	-	[34]
NiS/MoS2@N-rGO	Symmetric	6 M KOH	1028 $F.g^{-1}$ @1 $A.g^{-1}$	94.5/50000	[35]
VSL-MoS2@3D-Ni foam	Symmetric	Na_2SO_4/ PVA	34.1 $F.g^{-1}$@ 1.3 $A.g^{-1}$	82.5/10000	[36]
MoS_2/rGO	Symmetric	NaOH	323 $F.g^{-1}$ @ 0.2 $A.g^{-1}$	76.8/500	[37]
SS/MWCNTs/ $MoTe_2$	Symmetric	PVA-$LiClO_4$	68.01 $F.g^{-1}$ @ 0.2 $mA.cm^{-2}$	94/2000	[38]
MWCNTs/Mo Se_2	Symmetric	PVA-KOH	27 $F.g^{-1}$ @ 0.4 A/g	95/1000	[39]
MoS_2/carbon cloth	Symmetric	PVA-$LiClO_4$	368 $F.g^{-1}$ @ 5 mV/s	96.5/5000	[40]
MoS_2/NPG	Symmetric	1 M Na_2SO_4	102.5 F g^{-1} @ 1 A g^{-1}	91.67/5000	[41]
$(Ni,Co)_{0.85}Se$// porous graphene	Asymmetric	1.0 M KOH	529.3 mF c m^{-2} @ 1A g^{-1}	85/10000	[42]
MoS_2/PEI-GO	Asymmetric	Na2SO4	42.9 @ 0.5 A g^{-1}	93.1/8000	[43]
MoS_{2-x}@CNTs/Ni	Asymmetric	1 M Na_2SO_4	153.1F g^{-1} @ 1 A g^{-1}	91/3000	[44]

References

[1] F. Tavakoli, B. Rezaei, A.R. Taghipour Jahromi, A.A. Ensafi, Facile Synthesis of Yolk-Shelled $CuCo_2Se_4$ Microspheres as a Novel Electrode Material for Supercapacitor Application, ACS Applied Materials & Interfaces 12 (2019) 418-427.

[2] D. Sun, L. He, R. Chen, Y. Liu, B. Lv, S. Lin, B. Lin, Biomorphic composites composed of octahedral Co_3O_4 nanocrystals and mesoporous carbon microtubes templated from cotton for excellent supercapacitor electrodes, Applied Surface Science 465 (2019) 232-240.

[3] G. Li, Z. Chang, T. Li, L. Ma, K. Wang, Hierarchical Mn-Co sulfide nanosheets on nickel foam by electrochemical co-deposition for high-performance pseudocapacitors, Ionics 25 (2019) 3885-3895.

[4] F. Liao, X. Han, Y. Zhang, C. Xu, H. Chen, Solvothermal synthesis of porous $MnCo_2O_{4.5}$ spindle-like microstructures as high-performance electrode materials for supercapacitors, Ceramics International 44 (2018) 22622-22631.

[5] Z. Zhu, C. Han, T.-T. Li, Y. Hu, J. Qian, S. Huang, MOF-templated syntheses of porous Co_3O_4 hollow spheres and micro-flowers for enhanced performance in supercapacitors, CrystEngComm 20 (2018) 3812-3816.

[6] X. Hou, Y. Zhang, Q. Dong, Y. Hong, Y. Liu, W. Wang, J. Shao, W. Si, X. Dong, Metal organic framework derived core–shell structured Co9S8@ N–C@MoS_2 nanocubes for supercapacitor, ACS Applied Energy Materials 1 (2018) 3513-3520.

[7] R. Atchudan, T.N.J.I. Edison, D. Chakradhar, N. Karthik, S. Perumal, Y.R. Lee, One-pot dual product synthesis of hierarchical Co_3O_4@N-rGO for supercapacitors, N-GDs for label-free detection of metal ion and bio-imaging applications, Ceramics International 44 (2018) 2869-2883.

[8] P. Xu, W. Zeng, S. Luo, C. Ling, J. Xiao, A. Zhou, Y. Sun, K. Liao, 3D Ni-Co selenide nanorod array grown on carbon fiber paper: towards high-performance flexible supercapacitor electrode with new energy storage mechanism, Electrochimica Acta 241 (2017) 41-49.

[9] Y. Zhang, H. Xuan, Y. Xu, B. Guo, H. Li, L. Kang, P. Han, D. Wang, Y. Du, One-step large scale combustion synthesis mesoporous MnO_2/$MnCo_2O_4$ composite as electrode material for high-performance supercapacitors, Electrochimica Acta 206 (2016) 278-290.

[10] G. Sun, L. Ma, J. Ran, X. Shen, H. Tong, Incorporation of homogeneous Co_3O_4 into a nitrogen-doped carbon aerogel via a facile in situ synthesis method: implications for high performance asymmetric supercapacitors, Journal of Materials Chemistry A 4 (2016) 9542-9554.

[11] N.I. Chandrasekaran, H. Muthukumar, A.D. Sekar, A. Pugazhendhi, M.J.J.o.M.L. Manickam, High-performance asymmetric supercapacitor from nanostructured tin nickel sulfide ($SnNi_2S_4$) synthesized via microwave-assisted technique, 266 (2018) 649-657.

[12] J.S. Lee, C. Lee, J. Jun, D.H. Shin, J. Jang, A metal-oxide nanofiber-decorated three-dimensional graphene hybrid nanostructured flexible electrode for high-capacity electrochemical capacitors, Journal of Materials Chemistry A 2 (2014) 11922-11929.

[13] F. Zhu, M. Yan, Y. Liu, H. Shen, Y. Lei, W. Shi, Hexagonal prism-like hierarchical Co_9S_8@$Ni(OH)_2$ core–shell nanotubes on carbon fibers for high-performance asymmetric supercapacitors, Journal of Materials Chemistry A 5 (2017) 22782-22789.

[14] Y. Liu, J. Zhou, W. Fu, P. Zhang, X. Pan, E. Xie, In situ synthesis of CoSx@carbon core-shell nanospheres decorated in carbon nanofibers for capacitor electrodes with superior rate and cycling performances, Carbon 114 (2017) 187-197.

[15] H. Peng, G. Ma, K. Sun, Z. Zhang, J. Li, X. Zhou, Z. Lei, A novel aqueous asymmetric supercapacitor based on petal-like cobalt selenide nanosheets and nitrogen-doped porous carbon networks electrodes, Journal of Power Sources 297 (2015) 351-358.

[16] M. Qorbani, T.-c. Chou, Y.-H. Lee, S. Samireddi, N. Naseri, A. Ganguly, A. Esfandiar, C.-H. Wang, L.-C. Chen, K.-H. Chen, Multi-porous Co_3O_4 nanoflakes@ sponge-like few-layer partially reduced graphene oxide hybrids: towards highly stable asymmetric supercapacitors, Journal of Materials Chemistry A 5 (2017) 12569-12577.

[17] J. Li, C. Zhao, Y. Yang, C. Li, T. Hollenkamp, N. Burke, Z.-Y. Hu, G. Van Tendeloo, W. Chen, Synthesis of monodispersed $CoMoO_4$ nanoclusters on the ordered mesoporous carbons for environment-friendly supercapacitors, Journal of Alloys and Compounds 810 (2019) 151841.

[18] Y. Wang, W. Zhang, X. Guo, K. Jin, Z. Chen, Y. Liu, L. Yin, L. Li, K. Yin, L. Sun, Ni–Co Selenide Nanosheet/3D Graphene/Nickel Foam Binder-Free Electrode for High-Performance Supercapacitor, ACS applied materials & interfaces 11 (2019) 7946-7953.

[19] H. Fu, Y. Liu, L. Chen, Y. Shi, W. Kong, J. Hou, F. Yu, T. Wei, H. Wang, X. Guo, Designed formation of $NiCo_2O_4$ with different morphologies self-assembled from nanoparticles for asymmetric supercapacitors and electrocatalysts for oxygen evolution reaction, Electrochimica Acta 296 (2019) 719-729.

[20] P. Howli, S. Das, S. Sarkar, M. Samanta, K. Panigrahi, N.S. Das, K.K. Chattopadhyay, Co3O4 nanowires on flexible carbon fabric as a binder-free electrode for all solid-state symmetric supercapacitor, ACS omega 2 (2017) 4216-4226.

[21] X. Lu, X. Huang, S. Xie, T. Zhai, C. Wang, P. Zhang, M. Yu, W. Li, C. Liang, Y. Tong, Controllable synthesis of porous nickel–cobalt oxide nanosheets for supercapacitors, Journal of Materials Chemistry 22 (2012) 13357-13364.

[22] K. Gao, Z. Shao, J. Li, X. Wang, X. Peng, W. Wang, F. Wang, Cellulose nanofiber–graphene all solid-state flexible supercapacitors, Journal of Materials Chemistry A 1 (2013) 63-67.

[23] M. Gao, W.-K. Wang, Q. Rong, J. Jiang, Y.-J. Zhang, H.-Q. Yu, Porous ZnO-coated Co_3O_4 nanorod as a high-energy-density supercapacitor material, ACS applied materials & interfaces 10 (2018) 23163-23173.

[24] C. Guan, X. Liu, W. Ren, X. Li, C. Cheng, J. Wang, Rational design of metal-organic framework derived hollow $NiCo_2O_4$ arrays for flexible supercapacitor and electrocatalysis, Advanced Energy Materials 7 (2017) 1602391.

[25] J. Zhang, J. Lin, J. Wu, R. Xu, M. Lai, C. Gong, X. Chen, P. Zhou, Excellent electrochemical performance hierarchical Co_3O_4@Ni_3S_2 core/shell nanowire arrays for asymmetric supercapacitors, Electrochimica Acta 207 (2016) 87-96.

[26] S. Nagamuthu, K.-S. Ryu, Synthesis of Ag/NiO honeycomb structured nanoarrays as the electrode material for high performance asymmetric supercapacitor devices, Scientific reports 9 (2019) 1-11.

[27] C.-h. Tang, X. Yin, H. Gong, Superior performance asymmetric supercapacitors based on a directly grown commercial mass 3D Co_3O_4@$Ni(OH)_2$ core–shell electrode, ACS applied materials & interfaces 5 (2013) 10574-10582.

[28] K. Singh, S. Kumar, K. Agarwal, K. Soni, V.R. Gedela, K. Ghosh, Three-dimensional graphene with MoS_2 nanohybrid as potential energy storage/transfer device, Scientific reports 7 (2017) 1-12.

[29] J. Wu, J. Peng, Z. Yu, Y. Zhou, Y. Guo, Z. Li, Y. Lin, K. Ruan, C. Wu, Y. Xie, Acid-assisted exfoliation toward metallic sub-nanopore TaS_2 monolayer with high volumetric capacitance, Journal of the American Chemical Society 140 (2018) 493-498.

[30] X. Hu, W. Shao, X. Hang, X. Zhang, W. Zhu, Y. Xie, Superior Electrical Conductivity in Hydrogenated Layered Ternary Chalcogenide Nanosheets for Flexible All-Solid-State Supercapacitors, Angewandte Chemie International Edition 55 (2016) 5733-5738.

[31] R. Zeng, Z. Li, L. Li, Y. Li, J. Huang, Y. Xiao, K. Yuan, Y. Chen, Covalent connection of polyaniline with MoS_2 nanosheets toward ultrahigh rate capability supercapacitors, ACS Sustainable Chemistry & Engineering 7 (2019) 11540-11549.

[32] T.N. Khawula, K. Raju, P.J. Franklyn, I. Sigalas, K.I. Ozoemena, Symmetric pseudocapacitors based on molybdenum disulfide (MoS_2)-modified carbon nanospheres: correlating physicochemistry and synergistic interaction on energy storage, Journal of Materials Chemistry A 4 (2016) 6411-6425.

[33] Y. Jia, H. Wan, L. Chen, H. Zhou, J. Chen, Hierarchical nanosheet-based MoS_2/graphene nanobelts with high electrochemical energy storage performance, Journal of Power Sources 354 (2017) 1-9.

[34] H. Ji, S. Hu, Z. Jiang, S. Shi, W. Hou, G. Yang, Directly scalable preparation of sandwiched MoS_2/graphene nanocomposites via ball-milling with excellent electrochemical energy storage performance, Electrochimica Acta 299 (2019) 143-151.

[35] X. Xu, W. Zhong, X. Zhang, J. Dou, Z. Xiong, Y. Sun, T. Wang, Y. Du, Flexible symmetric supercapacitor with ultrahigh energy density based on NiS/MoS_2@N-rGO hybrids electrode, Journal of colloid and interface science 543 (2019) 147-155.

[36] R.K. Mishra, A.K. Kushwaha, S. Kim, S.G. Seo, S.H. Jin, Vertical-slate-like MoS_2 nanostructures on 3D-Ni-foam for binder-free, low-cost, and scalable solid-state symmetric supercapacitors, Current Applied Physics 19 (2019) 1-7.

[37] T. Xue, Y. Yang, X.-H. Yan, Z.-L. Zou, F. Han, Z. Yang, Free-standing and binder-free Molybdenum bisulfide nanospheres/reduced graphene oxide composite paper as flexible electrode for symmetric supercapacitor, Materials Research Express 6 (2019) 095029.

[38] S.S. Karade, B.R. Sankapal, Materials Mutualism through EDLC-Behaved MWCNTs with Pseudocapacitive $MoTe_2$ Nanopebbles: Enhanced Supercapacitive Performance, ACS Sustainable Chemistry & Engineering 6 (2018) 15072-15082.

[39] S.S. Karade, B.R. Sankapal, Two dimensional cryptomelane like growth of MoS_2 over MWCNTs: Symmetric all-solid-state supercapacitor, Journal of Electroanalytical Chemistry 802 (2017) 131-138.

[40] M.S. Javed, S. Dai, M. Wang, D. Guo, L. Chen, X. Wang, C. Hu, Y. Xi, High performance solid state flexible supercapacitor based on molybdenum sulfide hierarchical nanospheres, Journal of Power Sources 285 (2015) 63-69.

[41] S. Zhao, W. Xu, Z. Yang, X. Zhang, Q. Zhang, One-pot hydrothermal synthesis of nitrogen and phosphorus Co-doped graphene decorated with flower-like molybdenum sulfide for enhanced supercapacitor performance, Electrochimica Acta 331 (2020) 135265.

[42] C. Xia, Q. Jiang, C. Zhao, P.M. Beaujuge, H.N. Alshareef, Asymmetric supercapacitors with metal-like ternary selenides and porous graphene electrodes, Nano Energy 24 (2016) 78-86.

[43] M.-C. Liu, Y. Xu, Y.-X. Hu, Q.-Q. Yang, L.-B. Kong, W.-W. Liu, W.-J. Niu, Y.-L. Chueh, Electrostatically Charged MoS_2/Graphene Oxide Hybrid Composites for Excellent Electrochemical Energy Storage Devices, ACS Applied Materials & Interfaces 10 (2018) 35571-35579.

[44] P. Sun, R. Wang, Q. Wang, H. Wang, X. Wang, Uniform MoS_2 nanolayer with sulfur vacancy on carbon nanotube networks as binder-free electrodes for asymmetrical supercapacitor, Applied Surface Science 475 (2019) 793-802.